D. de Beer & M. Kühl (2001). Interfacial microbial mats and biofilms, pp. 374-394 In: B.P. Boudreau & B.B. Jørgensen (eds.), The Benthic Boundary Layer, Oxford University Press, New York, 2001.

15 INTERFACIAL MICROBIAL MATS AND BIOFILMS

Dirk de Beer

Michael Kühl

Biofilms and microbial mats can be defined as surface-associated layers of microbial cells embedded in extracellular polymeric substance (EPS; Characklis and Marshall, 1989; Stal and Caumette, 1994). Biofilms cover solid surfaces, while mats cover sediments. Biofilms range from a few cell layers to a maximum of a few mmillimeters in thickness, and microbial mats range from <1 mm to several centimeters in thickness. Furthermore, most microbial mats are characterized by high population densities of photoautotrophic microorganisms that act as primary producers in the top millimeters and build up the mat matrix, while many biofilms are heterotrophic and rely on substrate supply from the surface or the surrounding water. Despite these fundamental differences, biofilms and microbial mats share many characteristics, and both represent communities with complex strategies for microbial life at surfaces where steep gradients of physicochemical variables are found (chapters 8 and 14).

Mats cover sediments of shallow waters with calm hydrodynamics and little grazing by animals. Typically, these habitats exhibit extreme environmental conditions, and prolific mats develop, for example, in hot springs and hypersaline waters (Karsten and Kühl, 1996). Every surface, except perhaps healthy plant and animal epithelium, that is temporally or continuously wetted and is not exposed to nonphysiological conditions, creating environmental stress, is sooner or later covered by biofilm. Consequently, biofilms are almost everywhere, and in many shallow water ecosystems, biofilms and mats are responsible for the majority of the microbial conversions. In aquatic systems they cover sediment particles, rocks, and plants. Biofilms grow in pipelines and on ship hulls (increasing flow resistance and corrosion) and in heat exchangers (reducing heat transfer). They cover teeth (caries) and can colonize medical implants, possibly leading to incurable infections. Probably the most important practical use of biofilms is for biodegradation and bioremediation in bioreactors and in biologicalwaste water treatment plants.

Biofilms and microbial mats are thus important communities in most aquatic ecosystems both today and through geological time. For example, the first known fossils of individual microbes and communities share almost identical structural characteristics with those found in recent films and mats (Schopf and Klein, 1992).

Depending on growth conditions and age, the thickness of biofilms and mats can reach from a few microns to several centimeters, and the structural heterogeneity can be pronounced (figs. 15.1, 15.2). The active zones are typically in the order of a few millimeters or less. This poses a need for experimental techniques with a high spatial resolution, and microsensors have proven highly useful tools in the study of the biofilm/mat microenvironment and microbial activities (see chapter 8).

For modeling purposes and data analysis, the matrices have usually been assumed to be flat and impermeable for flow. However, recent findings in sediments (see chapter 7) and in biofilms (De Beer and Stoodley, 1995) indicate that careful analysis of this assumption is necessary. In this chapter we review some recent studies of mass-transfer phenomena (i.e., diffusion and advection), and their importance to metabolic processes in microbial mats and biofilms. In particular, we address the importance of integrating structural studies by microscopic techniques with microsensor analysis of transport and metabolic processes.

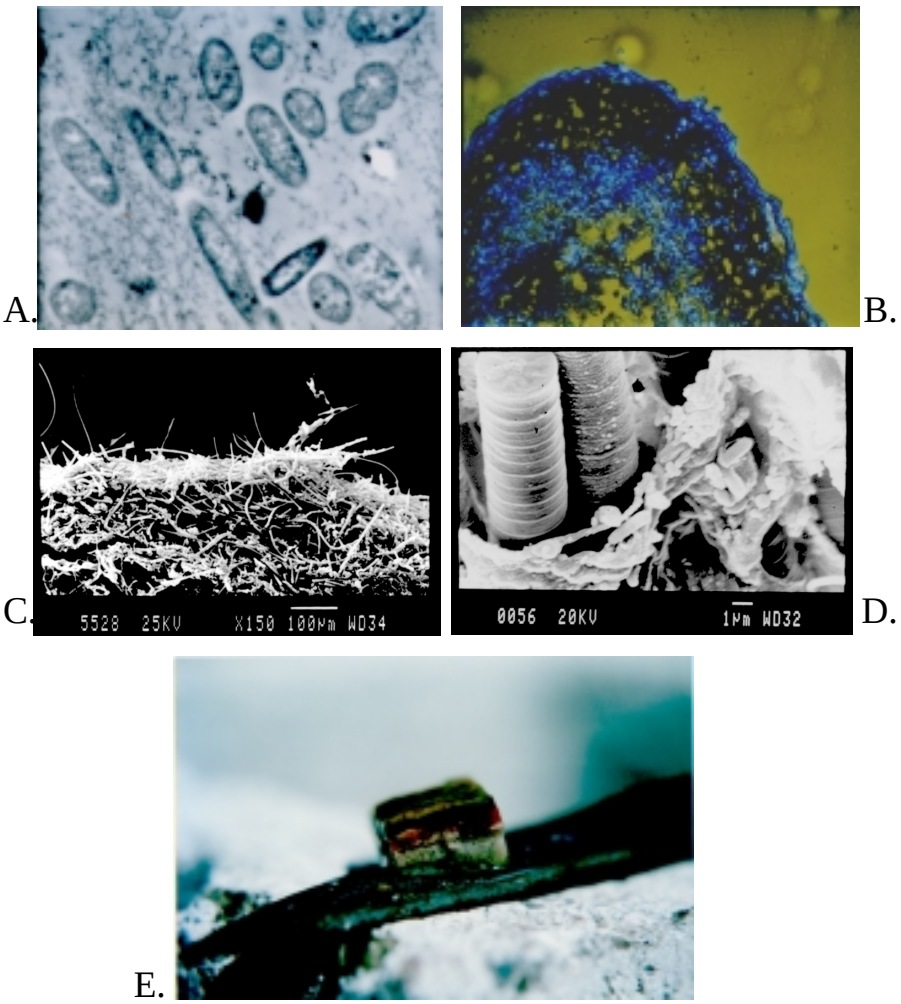

Figure 15.1 Examples of biofilms and microbial mats: A, Transmission electron microscopy (TEM) image of a biofilm section obtained from an anaerobic gas-lift reactor. The sample was stained with Ru-red to show EPS, visible as a dark netting between the cells. Scale bar = 1 µm. (From Beeftink and Staugaard, 1986, with permission). B, Section of methanogenic biofilm, EPS was stained with the fluorescent dye Calcofluor. The fluorescence distribution shows that the EPS, visible as bright blue, is present mainly in the top 50 µm. Scale bar = 100 µm. C,Top layer of a photosynthetic biofilm consisting of a dense network of filamentous cyanobacteria. D, The filaments are embedded in a matrix of EPS and bacteria. E, Example of a photosynthetic mat from a hot spring in Yellowstone Natinal Park in the United States. The brown and green layers contain unicellular cyanobacteria, while the red layer is dominated by phototrophic bacteria, *Chloroflexus* spp. (Karsten and Kühl, 1996). This last mat is about 1 cm in thickness. Color version available in the color insert of this book..

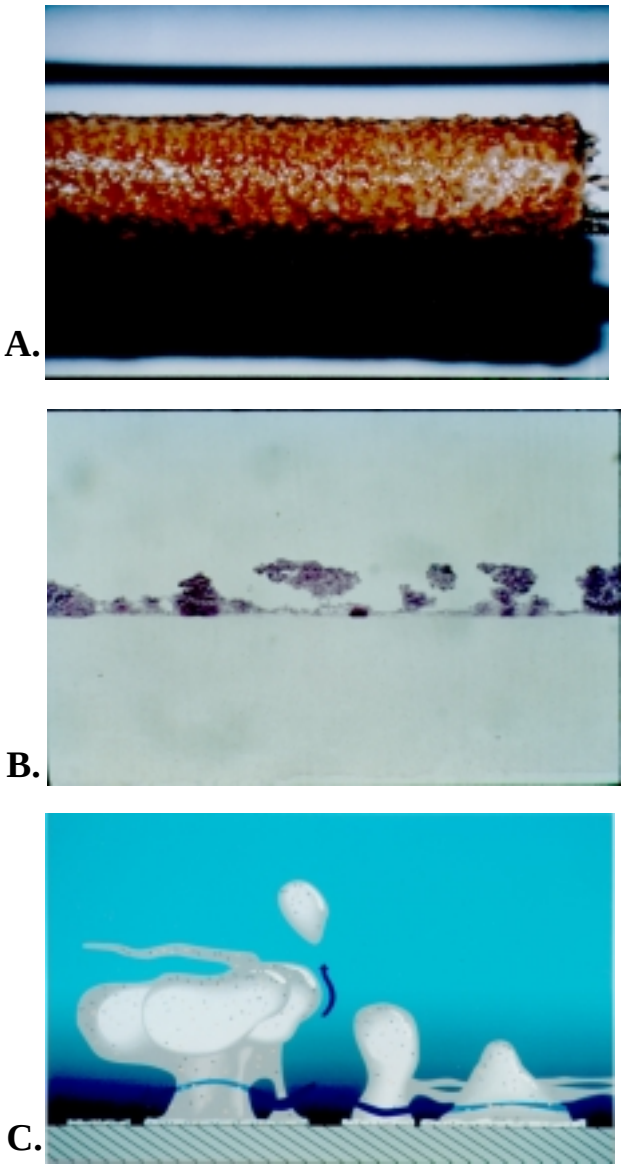

Figure 15.2 A, Macroscopic photograph of a 3–5 mm thick biofilm from a trickling filter used in gas treatment. (Curtesy of B. Ozinga, TUE, The Netherlands). B, Light microscopic image of a biofilm section, grown in a laboratory flow cell. This 200-μm-thick biofilm was stained with Crystal Violet. This image confirmed observations made by confocal scanning laser microscopy (CSLM), though artifacts are possible with this technique. C) Schematic of the biofilm structure, based on CSLM observations. Biofilms consist of a base film and cell clusters of various shapes, separated by voids. Cells can also aggregate into streamers. Color version available in the color insert of this book.

15.1 Structure and Composition of Biofilms and Mats

Biofilms and mats are matrices of cells and EPS. The EPS is produced by the cells and consists of polysaccharides, polyuronic acids, proteins, nucleic acids, and lipids (Decho, 1990; Decho and Lopez, 1993; Schmidt and Ahring, 1994). EPS cements the cells together and to the substratum. Due to the dimensions of microbial mats and biofilms, their structural analysis is strongly dependent on microscopic methods, which are briefly discussed below and listed in table 15.1 (see also chapter 6).

15.1.1 Techniques for Structural Analysis

Scanning electron (SEM), transmission electron (TEM), normal light (LM), fluorescence (FM), and confocal scanning laser microscopy (CSLM) are techniques that have been used most frequently to examine the structure and composition of biofilms and mats. Most microscopic methods involve preparation of the sample, including staining, fixation, freezing, dehydration, embedding and sectioning. The target matrices are soft and consist of >95% water (Christensen and Characklis, 1990). Preparations for microscopy can strongly change the matrix structure by shrinking and deformation, and the resulting artifacts have influenced the concept of biofilm structure for years. Most relevant is the underestimation of the spatial heterogeneity, as preparations tend to smooth the soft biofilm structures.

Only atomic force microscopy (AFM), environmental scanning electron microscopy (ESEM), and CSLM allow examination of unfixed samples. The recent application of CSLM has changed our concept of biofilm/mat structure completely (Lawrence et al., 1991; De Beer et al., 1994b; Massol-Deya et al., 1995). With this technique, living transparent tissues can be sectioned optically, under growth conditions. An excellent description of confocal microscopy techniques was published by Lawrence et al. (1991).

15.1.2 Staining of Structural Components

Specific staining is an important tool for unraveling the spatial distribution of different biofilm components, of which cells and EPS are most significant. For nonspecific DNA stains such as acridine orange, diamidino-phenylindole (DAPI), ethydium bromide, and hexidium iodide are most useful (see table 15.2). These dyes can be combined with CSLM to give an image of cell distributions in undisturbed biofilms/mats. Species-specific staining is also possible with antibodies and molecular probes. The latter technique is promising but is not discussed here, as it has little relevance to the visualization of biofilm architecture, because embedding and dehydration are required during the staining procedure.

Much less attention has been paid to visualization of EPS. Specific staining for fluorescent microscopy or CSLM is possible for proteins (fluorescein iso-thiocyanate), polyuronic acids, and polysaccharides (lectin conjugates, calcofluor). EPS dyes will also stain cells that become visible as discrete points, while EPS is visible as a continuous sheet. For further information on fluorescent staining techniques, see Haugland (1996). EPS can also be stained by Ru-red for TEM, or observed directly by SEM. EPS appears then as strands connecting the cells (fig. 15.1). EPS morphology changes with dehydration: diffuse polymeric matter is condensed to strands leading to overestimation of the pore size. From SEM images the pore size appears to be in the order of 1 μm. The TEM preparation in figure 15.1A shows a pore size of a few hundred nanometers. Images acquired by ESEM (Little et al., 1991) and AFM (Bremer et al., 1992) with submicron resolution (no dehydration), do not show these strands, but rather shown a smooth smear. Possible artifacts in ESEM include filling of recesses

Table 15.1 List of microscopic techniques for studying biofilm and mats

Microscopy Technique	Spatial Resolution	Application	Sample Treatment	References
LM	1 μm	Polymers and cells	Dehydration, freezing, sectioning, staining	Chayen et al. (1973)
FM	1 μm	Polymers and cells	Dehydration, freezing, sectioning, staining	Stewart et al. (1995) Griebe (1991)
SEM	1 nm	Cell and polymer surfaces	Dehydration, sputter coating	Beeftink and Staugaard (1986)
ESEM	10 nm	Cell and polymer surfaces	None	Little et al. (1991)
TEM	1 nm	Cells and polymers	Dehydration, sectioning, staining	Beeftink and Staugaard (1986)
CSLM	1 μm	Polymers, cells, voids	Staining	Lawrence et al. (1991) De Beer et al. (1994b)
AFM	0.1 μm	Cell and polymer surfaces	None	Bremer et al. (1992)

Table 15.2 Dyes for structural analysis of biofilms and microbial mats

Structure	Dye	Microscopy	Staining
Cells	Classical stains (Crystal violet, Gram stains etc.)	LM	All cells
	Acridine orange DAPI	FM and CSLM	All cells
	Ethidium bromide Eropidium iodide	FM and CSLM	Dead cells
	Hexidium iodide	FM	Living cells
	CTC, formamide	FM and CSLM	Respiratory active cells
Voids and channels	Dextran conjugate	FM	Voids
	Beads	FM and CSLM	Voids
	Fluorescein	CSLM	Voids
EPS	Alcian bleu	LM	EPS (carbohydrates)
	Lectins	FM and CSLM	EPS (carbohydrates)
	Calcofluor	FM and CSLM	EPS (carbohydrates)
	Fluoroscein isothiocyanate (FITC)	FM and CSLM	EPS (proteins)
	Heavy metals	TEM	Cells, EPS

with water, "drowning" the roughness elements of the surface. The sensor needle of the AFM might disturb the surrounding water, causing the polymers to move and resulting in a blurred image.

EPS is cross-linked, which is important since the polymers are not dissolved and do not increase the viscosity of the interstitial water. EPS can be considered as a solid sponge with high water content. (The transport properties of such a matrix and their relation to the matrix micro-structure are discussed in a later section.) In conclusion, several new techniques now make it possible to achieve a much more detailed view of biofilm/microbial mat structure. Some of these techniques need, however, further optimization for use in heavily pigmented microbial mats, which exhibit a strong light attenuation and a high autofluorescence.

15.1.3 Case Study of a Model Biofilm

Most researchers assume biofilms to be flat, an assumption that is often supported by microscopic observations. However, some authors using TEM and LM observe biofilms that contain voids, channels, and pores, with cells arranged in clusters, streamers, colonies, or layers (Mack et al., 1975; Eighmy et al., 1983; Robinson et al., 1984; Kugaprasatham et al., 1992; Stewart et al., 1995). These voids are thought to act as transport channels (Robinson et al., 1984; Kugaprasatham et al., 1992), without supporting evidence. Lawrence et al. (1991) pioneered CSLM studies on thin monospecies biofilms (30 μm). They used negative staining by fluorescein, a nontoxic, nonbinding, small molecule whose fluorescence is quenched in the presence of biomass. This latter work confirmed that biofilms are heterogeneous with voids of 10–20 μm (>50% of biofilm volume).

These structures were also observed with CSLM in mixed-culture biofilms, grown under higher flow conditions and reaching thicknesses of up to 600 μm (Stewart et al., 1993, 1995; De Beer et al., 1994b). An extensive analysis was done on biofilms grown in a flow cell with an observation window on the top, allowing in situ CSLM observations on the growing biofilm. In these biofilms the cell clusters were 150–300 μm in diameter and voids were ~100 μm wide. Staining techniques included cell staining with DAPI and acridine orange, negative staining with fluorescein, and EPS staining with calcofluor and alcian blue. The results showed that cells and EPS were exclusively present in cell clusters and that voids were really empty. Fluorescent beads added to the bulk liquid almost instantaneously penetrated the voids. This showed that the voids are in open connection with the bulk liquid and exchange their contents rapidly. From these observations a new concept of biofilm structure emerged, a base film of 10–30 μm, cell clusters (150–300 μm) and voids (100 μm, as schematically presented in figure 15.2C This structure was, with some difficulty, also shown by classical microscopy techniques (taining with Crystal Violet; fig. 15.2B). A very similar structure was found using CSLM for biofilms from a wastewater treatment plant (Massol-Deya et al., 1995). The considerable amount of void space in a biofilm might allow internal flow and advective exchange between the biofilm and the bulk liquid.

Although the results obtained by CSLM were taken as proof of biofilm heterogeneity, studies of biofilm architecture can be done without it. Often the heterogeneity is on a rather large scale with voids and cell clusters of the order of 0.2–1 mm. Then the relevant structures can be seen with a dissection microscope or the unaided eye. Such a biofilm structure is streamers, which can be seen with the naked eye. Streamers are filaments that are millimeters to centimeters in length and attached to the biofilm surface. In contrast to cell clusters, streamers are flexible and move freely in the flow.

In summary, three types of biofilm growth can be defined: flat, clustered, or with streamers. Within one biofilm all these types can coexist: a flat base film covered with clusters to which streamers are attached. Tijhuis et al. (1996) suggested that the degree of heterogeneity is determined by the balance between the growth and abrasion

rates. Indeed, slow-growing organisms (e.g., nitrifiers and methanogens) form relatively flat biofilms or spherical aggregates, while faster growing heterotrophs produce more heterogeneous biofilms with cell clusters and streamers. We speculate that cell surface properties, in particular hydrophobicity or hydrophilicity, can also determine the biofilm structure. Cell surface hydrophobicity results in minimization of the contact surface between liquid and biofilm and thus favors planar biofilms or spherical aggregates. Hydrophilic cells will more easily form protrusions such as streamers and cell clusters. Typically, dividing cells (Allison et al., 1990) and many facultative aerobic heterotrophs (Daffonchio et al., 1995) are hydrophilic. Heterotrophic conditions thus result in heterogeneous biofilms. Examples of hydrophobic microorganisms are benthic cyanobacteria (Fattom and Shilo, 1984), methanogens, syntrophic bacteria, and to a lesser extent, sulfate reducers (Daffonchio et al., 1995). Indeed, cyanobacterial mats and methanogenic biofilms are usually relatively flat; however, detailed observations on mat structure and heterogeneity are lacking.

Finally, cell-cell communication must be considered as a morphogenetic mechanism. By sensing cell-produced compounds (e.g., acyl-homoserine lactones, where the acyl group determines action or strain specificity) cells recognize the local cell density, so-called *quorum sensing*, and react by switching on or off certain sets of functional genes. For example, quorum sensing regulates the expression of the *Lux* genes in the bioluminescent bacterium *Vibrio fisheri*, it regulates the release of virulence genes in pathogens such as *Pseudomonas aeruginosa*, and plays a role in the symbiotic host association of *Rhizobium leguminosarum* in root nodules. Genes for quorum sensing have been found in about 25 different bacterial species, and this communication mechanism is believed to be common among gram-negative bacteria (Greenberg, 1997).

Quorum sensing also determines the structure of *P. aeruginosa* biofilms (D.G. Davies, personal communication). Presence of N-3-oxododecanoyl-L-homoserine lactone enhances the production of polyuronic acids, which are important components of bacterial EPS. The lactone concentration is increased at higher cell densities or after adhesion to a surface due to restricted outdiffusion, thus (auto)stimulating biofilm formation. At higher concentrations, as can occur in dense and thick biofilms, the same compound induces production of N-butyryl-L-homoserine lactone, which then induces the production of alginate lyase that can dissolve EPS and lead to rapid cell mobilization and formation of voids in the biofilm matrix. Mutants of *P. aeruginosa* with a defect in quorum sensing form flat and homogeneous biofilms, while the wild-type forms heterogeneous biofilms (Davies et al., 1998). If these mutants are grown in a medium with added N-3-oxododecanoyl-L-homoserine lactone, a patchy biofilm resembling that seen in nature is formed. Biofilm structure can thus be regulated by two counteracting lactones, one that stimulates cell aggregation and biofilm formation, and another that stimulates biofilm dissolution.

15.2 Function of Biofilms and Microbial Mats

A common property of microbial mats and biofilms is the occurrence of mass-transfer resistance from limited water flow inside the matrix and the presence of a hydrodynamic boundary layer between the matrix and the surrounding turbulent water (Jørgensen and Revsbech, 1985; Jørgensen, 1994). Transport of solutes is thought to be primarily diffusional inside the matrix and in the boundary layer adjacent to the solid surface (for a more fundamental discussion of boundary layers and diffusion in a porous medium, see chapters 5, 9 and 14; Boudreau, 1997). Consequently, the internal chemical composition differs from the bulk-water conditions with respect to substrates and products, and steep gradients can develop. This has strong effects on the type of microbial conversions that occur and their rates.

Conversions are often limited by mass-transfer resistance; however, many processes can only occur inside the biofilms because of special prevailing conditions. For exam-

ple, anaerobic conversions such as denitrification, sulfate reduction, and methanogenesis take place primarily in the anoxic environments found in the deeper zones of biofilms and mats. Nevertheless, recent studies have shown that anaerobic processes also can occur in the oxic part of sediments and mats, indicating that special physiological adaptations of anaerobic bacteria and anaerobic microniches may exist in the oxic zone (Canfield and Des Marais, 1991; Frund and Cohen, 1992; Krekeler et al., 1997). A characterization of these microenvironments and their interaction with mass-transfer processes is needed in order to understand conversions inside mats and biofilms.

The simplest biofilm model is that of a planar geometry with microbial activity distributed homogeneously and all transport parameters constant throughout the mat. Transport inside the film is diffusional. Adjacent to the biofilm is a boundary layer in which the transport gradually changes from molecular to turbulent diffusion in going toward the mixed bulk liquid (see chapter 5). The main attraction of this concept is its simplicity which facilitates mathematical modeling of transport, conversion, and growth (Wanner and Gujer, 1986; Rittmann and Manem, 1992). Below, we estimate the relative importance of the *diffusive boundary layer* (DBL) to biofilm or mat processes in this ideal planar geometry, using an engineering-type approach.

15.2.1 Role of Boundary Layers

Mass-transfer resistances can be separated into that of the DBL and that in the matrix itself. The resistance in the DBL is proportional to its thickness which depends mainly on the flow speed (Jørgensen and Des Marais, 1990). The resistance in the matrix is determined by the effective diffusion coefficient and the penetration depth (diffusion distance) of the limiting substrate. The relative importance of the DBL and intramatrix resistance to conversion rates can be found for flat geometry with first- and zero-order kinetics. Both are present here, because microbial kinetics are of mixed-order saturation type, that is, *Monod kinetics*, which are zero-order for high substrate concentration and first-order for low substrate concentration. Bailey and Ollis (1986) give an analysis for first-order kinetics. The effect of internal mass-transfer resistance on the effectiveness factor, η, of a flat porous catalyst is given by

$$\eta = \frac{\tanh(\phi)}{\phi} \tag{15.1}$$

where ϕ is the first-order Thiele modulus:

$$\phi = L_b \sqrt{\frac{k}{D_b}} \tag{15.2}$$

where L_b is the biofilm/mat thickness, k is the first-order reaction-rate constant, and D_b is the *effective diffusion coefficient*. The *Thiele modulus*, ϕ, is the square root of the ratio of first-order reaction rate ($L_b^3 k c_o$) and diffusion rate ($L_b D_b c_o$), where c_o is the concentration of the solute at the biofilm/mat top surface.

If, in addition, external mass-transfer resistance is included, then the total effectiveness factor, η_t, is given by

$$\eta_t = \frac{\tanh(\phi)}{\phi\left(1 + \dfrac{\phi \tanh(\phi)}{\mathrm{Bi}}\right)} \tag{15.3}$$

where Bi is the *Biot number* defined as

$$\mathrm{Bi} = \frac{\text{characteristic external mass transfer rate}}{\text{characteristic internal mass transfer rate}} = \frac{\beta L_b}{D_b} \tag{15.4}$$

where β is the *mass-transfer coefficient* for the DBL (see chapter 5).

The effecst of different resistances on η_t appear with rearrangement of equation 15.3:

$$\frac{1}{\eta_t} = \frac{1}{\eta} + \frac{\phi^2}{\mathrm{Bi}} \tag{15.5}$$

Here, the first term reflects the internal mass-transfer resistance, due to diffusion and reaction in the biofilm/mat, and the second term represents the external resistance from the DBL. The ratio of η to η_t,

$$\frac{\eta\phi^2}{\mathrm{Bi}} = \frac{k L_b}{\beta} \tag{15.6}$$

expresses the relative importance of the DBL to the conversion rate. If the ratio is much smaller than 1 (typical for rather inactive systems with low *k* and subjected to flow), the resistance from the DBL can be ignored. If the ratio is much greater than 1, then the DBL resistance determines the conversion rate. If the ratio is of order unity, both resistances must be considered. Furthermore, if Bi > 100 ,boundary-layer (external) mass-transfer resistance can be ignored.

The mass-transport coefficient, β, can be calculated from the hydrodynamics as described in chapter 5. For example, from Shaw and Hanratty (1977),

$$\beta = 0.0889\, u_* \, \mathrm{Sc}^{-0.704} \tag{15.7}$$

where u_* is the *shear velocity* (see chapter 2) and Sc is the *Schmidt number*, μ/D, where μ is the *kinematic viscosity* and *D* is the *molecular diffusion coefficient*.

For biological conversions, a zero-order approach is often more realistic, as the saturation concentration, K_m, for microbial conversions is often low (e.g., Boudreau and Westrich, 1984). For zero-order kinetics, the bulk and surface concentrations , (i.e., c_b and c_0, respectively) have to be taken into account, and one has to differentiate between full and partial penetration of the biofilm, that is, whether the solute is consumed before it can penetrate to the base of the biofilm/mat. The biofilm is fully penetrated with zero-order kinetics if

$$\phi_0 = L_b \sqrt{\frac{k_0}{D_b c_0}} \le \sqrt{2} \tag{15.8}$$

where ϕ_0 is called the zero-order *Thiele modulus*. At full substrate penetration and zero-order kinetics, conversion is not limited by mass transfer, that is, it is a fixed quantity set by the zero-order kinetics. Thus, further analysis on the dominance of the resistances is unnecessary.

At partial penetration and zero-order kinetics, ($\phi_0 > \sqrt{2}$) the flux is given by

$$j = \beta(c_b - c_0) = k_0 \ell_p = k_0 \sqrt{\frac{2 D_b c_0}{k_0}} \tag{15.9}$$

where ℓ_p is the *substrate penetration depth*. With equations 15.7 and 15.9, c_0 can now

be calculated, and Bi is given by

$$Bi = \frac{k_s L_b}{D_b} = \frac{k_0 L_b \sqrt{\frac{2D_b c_0}{k_0}}}{(c_b - c_0)D_b} = \frac{c_0}{c_0 - c_b}\sqrt{2}\phi_0 \qquad (15.10)$$

Again, external resistance is insignificant if Bi ≥ 100. When Bi applies only to the active layer, then:

$$Bi^* = \frac{k_s \ell_p}{D_b} = \frac{k_0 \ell_p^2}{D_b(c_b - c_0)} = \frac{k_0 \ell_p^2}{D_b c_0}\frac{c_0}{c_b - c_0} = 2\frac{c_0}{c_b - c_0} \qquad (15.11)$$

These latter equations are useful for sediments that can be assumed to be infinitely thick. In table 15.3 the Biot number is calculated for a few systems, ranging from a very active nitrifying biofilm to a rather inactive deep-sea sediment. The starting data for the calculations were microprofiles obtained with O_2 microsensors. The values for β were calculated from D_b/δ_d (see eq. [5.17]), the values for k_0 were obtained from j/ℓ_p. The values of j and δ_d were determined graphically, the inaccuracy of which explains the small differences between Bi*I and Bi*II. The examples in table 15.3 show that the effect of the boundary layer on the microbial conversions in sediments is more strongly determined by the variations in volumetric activity than the boundary-layer thickness.

15.2.2 Diminution of Mass-Transfer Resistance

Mass-transfer resistance from boundary layers imposes some constraints on the metabolic activity within biofilms and microbial mats. The external supply of substrates for growth may determine the productivity of these communities, while impeding the transport of metabolic products that may have inhibitory or damaging effects. Microbes, thus, must adapt to these conditions (see also chapter 14).

While oxygen consumption is limited by the boundary layer in most heterotrophic biofilms and mats (Jørgensen and Revsbech, 1985; Jørgensen and Des Marais, 1990), this mass-transfer resistance can be alleviated in photosynthetic systems by the internal oxygen production, which supersaturates the photic zone and pushes the oxic-anoxic interface deeper (Kühl et al., 1996). During photosynthesis carbon dioxide is fixed, leading to a pH increase; carbon dioxide can become a limiting substrate for photosynthesis, if it is primarily supplied across the DBL from the overlying water (De Beer et al., 1997a). Furthermore, the resulting high ratio of oxygen to carbon dioxide can increase photorespiration and photoinhibition.

In addition, nutrient supply from the overlying water may limit productivity. By pushing the oxic-anoxic interface to greater depths below the surface, anaerobic processes that depend on substrate supply from the water may also be indirectly affected by the increased diffusion path from the water to the depth of activity in the light. Assimilation of necessary substrates in the photic zone may also be an impediment. Both mechanisms were shown to be important regulating factors for denitrification in a photosynthetic freshwater biofilm (Nielsen et al., 1990). The overall denitrification rate was primarily a function of the light-dependent thickness of the aerobic layer below which denitrification occurred, that is, the diffusion path-length for nitrate from the water to the reaction zone. Microaerophilic and anaerobic organisms living around the oxic-anoxic interface consequently find themselves under pressure to either stay put and cope with unfavorable conditions during, or to move to a more optimal position, in response to the chemical and physical gradients present (see chapter 14).

Table 15.3 Biot numbers for a range of films, mats, and sediments.

	k_0	β	ℓ_p	D_e	δ_d	j	**Bi*I**	**Bi*II**
A	2.88E-02	9.00E-06	0.0001	2.70E-09	0.0003	2.88E-06	**0.333**	**0.761**
B1[a]	1.33E-02	5.67E-06	0.00005	2.55E-09	0.00045	6.67E-07	**0.11**	**0.11**
B2[a]	1.00E-02	1.70E-05	0.00015	2.55E-09	0.00015	1.5E-06	**1**	**1.15**
C	4.29E-04	1.44E-06	0.0007	1.44E-09	0.001	3.00E-07	**0.7**	**0.66**
D	6.50E-05	1.44E-06	0.002	1.44E-09	0.001	1.30E-07	**2**	**1.8**
E[b]	2.58E-08	1.55E-06	0.12	1.24E-09	0.0008	3.1E-09	**150**	**149.6**

Nitrifying biofilm(A; De Beer et al., 1993), microbial mats (B; Jørgensen and Des Marais, 1990), silty (C)and sandy (D) lake sediment (Sweerts et al., 1991), and deep-sea sediments in an upwelling area off the Chilean coast (E; 4073 m depth). *Biot numbers*, Bi, are calculated from microprofiles in two ways.

$$\text{Bi*I} = \frac{\beta \ell_p}{D_b} \qquad \text{and} \qquad \text{Bi*II} = \frac{k_0 \ell_p^2}{D_b (c_b - c_0)}$$

δ_d is the DBL thickness, and all units are SI.

[a] Flow velocity 0.3 cm s^{-1} (B1) and 7.7 cm s^{-1} (B2).

[b] Data kindly supplied by Ola Holby (MPI, Bremen), Jens Gundersen, and Ronnie Glud (University of Aarhus, Denmark).

Besides the above cited disadvantages, the close coupling between autotrophs and heterotrophs in biofilms and mats possibly allows for a very efficient cross-feeding between these two components, thus leading to an internal cycle of electron donors and acceptors within the system (Canfield and Des Marais, 1993; Kühl et al., 1996). Consequently, such systems may depend much less on the external supply as expected from the high metabolic activity found in biofilms and mats. The net growth rate of such systems is low as a result of this efficient cycling between production and remineralization. While this may hold true for photosynthetic biofilms and mats, heterotrophic biofilms exhibit a much more pronounced dependency on external supply and can grow very fast under favorable conditions. At the same time, such biofilms tend to become more heterogeneous than photosynthetic biofilms and mats, which,in many cases where pronounced bioturbation is absent can be described reasonably well with 1D geometry, assuming a high degree of lateral homogeneity.

The simplification to 1D diffusional transport is convenient for modeling, but not always justified. Mathematical modeling can lead to incorrect results if the reality is more complex than the assumptions on which the model is based. Thus, model assumptions should be checked. The use of experimental techniques with a high spatial resolution can give insight into mass-transfer phenomena and microenvironments. This was first shown by Jørgensen and Des Marais (1990), who mapped the surface topography and the properties of the DBL above a microbial mat. The upper boundary of the DBL was shown to follow closely the surface topography of the mat, and the DBL thickness varied significantly within a 1 cm^2 mat area (see fig. 14.7 in chapter 14). Taking this surface topography effect into account, the calculated oxygen flux across the mat-water interface was increased by about 50% relative to the 1D diffusion flux calculated from vertical oxygen micro-gradients. This example clearly illustrates the importance of taking heterogeneity into account when investigating mass transfer and mass-transfer-dependent biological conversions in natural communities. The following section discusses another example wherein detailed studies of biofilm structure and mass-transfer measurements were combined.

15.2.3 Measurements in a Model Biofilm

The assumption that transport inside the biofilm is purely diffusional is challenged by the observation of voids in biofilms (fig. 15.2C). This situation was investigated by De Beer et al. (1994a) using a model biofilm grown in the flow cell. The presence of flow inside the voids was first tested by microinjection. A 10 μm micropipette filled with a fluorescein solution was positioned in either a cell cluster or a void. A plume developed when fluorescein was injected slowly. In a flowing liquid the plume becomes elongated, with the ratio of width to length increasing with flow velocity. In the voids the plume elongated with increasing bulk flow. In the cell clusters the ratio remained at 1, regardless of the bulk flow. Thus, in voids liquid can flow, and in cell clusters liquid is always stagnant. Consequently, both advective transport and diffusion are possible in voids, while in cell clusters diffusion is the only transport mechanism. Unfortunately, quantification of flow is not possible with this technique.

To record flow profiles we used particle tracking with confocal microscopy. The particles were neutrally buoyant fluorescent latex beads. The narrow focal plane (20 μm) observed by confocal microscopy allows precise depth location of the moving beads. At low flow velocity individual beads were tracked by capturing sequences of images. At higher velocities the beads appear as streaks in the image and velocity was determined from the streak length and the scan speed. Flow velocity profiles were recorded at different bulk flow velocities. These profiles (fig. 15.3) make clear that flow occurs inside the biofilm with a velocity that is proportional to the bulk flow. The flow profile inside the biofilms is more or less linear, and liquid is stagnant only at the base of the biofilm. Shear forces can be calculated from the flow profiles (fig. 15.4).

Comparison of the situation with and without biofilm shows clearly that the presence of the biofilm influences the flow inside the flow cell only at Re_r (i.e., *roughness Reynolds number*) higher than 5, where

$$Re_r = \frac{\rho u_\infty z_0}{\mu}\left(\frac{C_f}{8}\right)^{0.5} \tag{15.12}$$

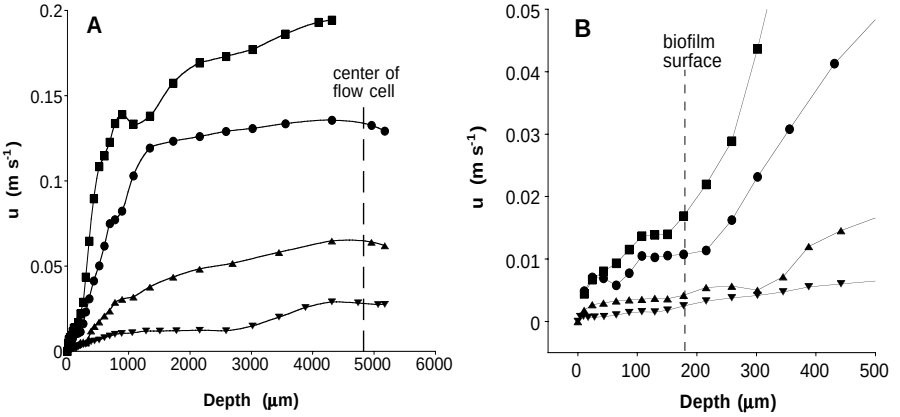

Figure 15.3 Velocity profiles measured with particle tracking and CSLM. Particles were neutrally buoyant fluorescent latex spheres (0.3, 1, and 23 μm diameters; at larger distances from the lens, larger spheres are needed). A illustrates half the profiles, down to the center of the flow cell, around which the profiles were symmetrical. B is an enlargement of the origin showing profiles inside the biofilm. Measurements were done at a bulk flow velocities (in m s–*1*) of 0.164 (■), 0.102 (●), 0.034 (▲) and 0.011 (▼).

where ρ is the fluid density, z_0 is the roughness height, u_∞ is the bulk flow velocity, and C_f is the friction factor. This latter dimensionless number is used to evaluate the hydraulic regime near rough surfaces. At $Re_r < 5$, for this case study if the bulk flow velocity $u_\infty < 0.1$ m s^{-1}, the regime is considered smooth (Schlichting, 1968), in agreement with our results.

Particle tracking shows unambiguously that flow occurs inside the biofilm with a magnitude proportional to the bulk flow velocity. Still unanswered is whether the intrabiofilm flow resulted in increased substrate mass transport; that is, diffusion may still be dominant.

Specifically, if the voids act as transport channels, then the substrate concentration inside the voids must be higher than in the adjacent cell clusters. This point was studied by De Beer et al. (1994b) using oxygen microsensors. In this case, the biofilm grew subject to oxygen limitation. Under microscopic guidance microsensors were positioned inside the voids or cell clusters. Profiles were measured in the vertical direction and contour plots were constructed from profiles measured along transects. During growth conditions the oxygen concentration inside the voids was indeed higher than in the cell clusters. Oxygen penetrated only 50 μm into the 170–200-μm-thick cell clusters, but penetrated the voids to the substratum (fig. 15.5). Due to the concentration difference, oxygen can diffuse from the voids into the cell clusters; in other words, voids act as transport channels supplying the cell clusters with substrate. This point is made clearer with the aid of contour plots (fig. 15.6) of oxygen isopleths. Under growth conditions ($u_\infty = 0.064$ m s^{-1}), the oxygen contours follow the surface of the solid biomass, and the steepest gradients are present at the cell cluster surface. A considerable horizontal component is present especially at the side of the cell clusters in the voids. Clearly a 1D approach is inadequate to describe the oxygen distribution inside the biofilm.

Since advection inside the biofilm is driven by bulk flow, the voids will act less as transport channels at lower flow velocities. Indeed at $u_\infty < 0.01$ m s^{-1} the oxygen profiles in the voids become identical to those in the cell clusters. Contour plots show that the isolines then do not follow the irregular biofilm surface, but are more or less flat.

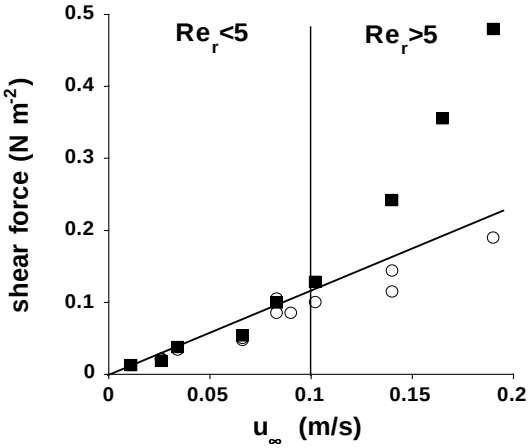

Figure 15.4 Effect of biofilm presence on shear force. The shear forces were calculated from flow profiles measured by particle tracking. At a smooth surface without biofilm (open circles) the shear force is accurately described by the theoretical (solid line). At the surface of an irregular biofilm (■) the shear forces increase strongly above $Re_r = 5$.

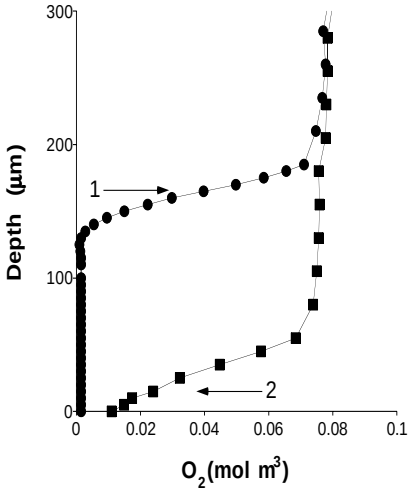

Figure 15.5 Oxygen microprofiles measured in a heterogeneous biofilm, growing in a flow cell. Profiles were measured under growth conditions in a void (■) and above a cell cluster (●). Arrows indicate the surface of the cluster (1) and the base film (2).

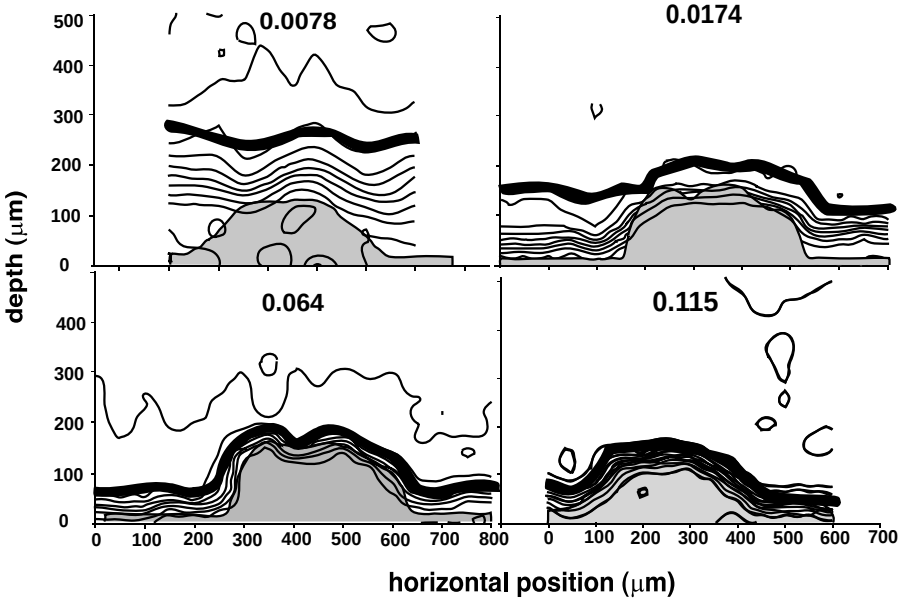

Figure 15.6 O_2 distribution in a heterogeneous biofilm, measured at different u_∞ values, as indicated in each plot (in m s^{-1}). The thin lines are the isopleths connecting equal O_2 concentrations; the thick line indicates the upper limit of DBL, δ_d. The gray areas represent the biomass (cell clusters and base film).

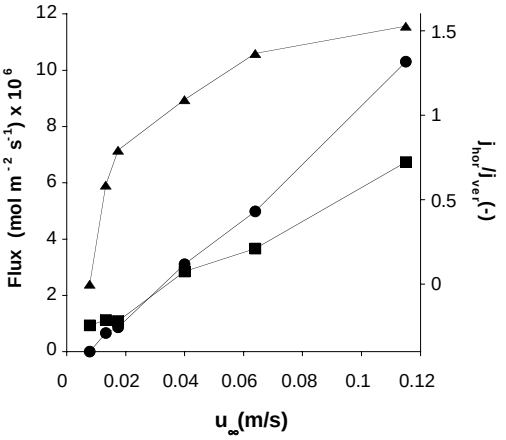

Figure 15.7 Oxygen fluxes into the model biofilm at different u_∞. Fluxes from the voids ($j_{horizontal}$) and directly from the bulk liquid ($j_{vertical}$) are plotted as well as their ratio.

The upper limit of the hypothetical DBL, δ_d, which represents the effective exchange surface between biofilm and bulk, is horizontal. The biofilm can be considered as planar with respect to its effect on transport. Above 0.03 m s^{-1}, the DBL follows the irregular biofilm surface, and mass transport must be treated as a 3D phenomenon. The consequences for the mass-transfer rate are shown in figure 15.7. The fluxes in vertical and horizontal direction are plotted against the bulk flow velocity. Above a velocity of 0.03 m s^{-1}, the horizontal component is more important than the vertical component, and only below 0.01 m s^{-1} can the horizontal component be ignored. The presence of voids increases the total flux up to 2.5 times.

The biofilm is hydraulically smooth below 0.1 m s^{-1} (fig. 15.4), but for mass transfer it is smooth below about 0.01 m s^{-1} (fig. 15.7). This means that liquid flow and mass transfer are not equally influenced by the film rough. Consequently, Re_r cannot be used to judge whether roughness has increased the effective exchange area. Data in De Beer and Stoodley (1995) indicate that a 3D approach is needed when δ_d is about 30% of the size of the irregularities of the biofilm. (For calculation of δ_d for a rough surface, see chapter 5).

15.2.4 Diffusional Mass Transfer in Biofilms and Mats

Mass transfer by advection is much more efficient than by diffusion. However, diffusion is the mode of transport in many biofilms, at least in the cell clusters, and it is assumed to dominate transport in microbial mats. Measurements in different biofilms report D_b values varying from 1% to 900% of the diffusion coefficient in water (Libicki et al., 1988). This reflects not only the variety of biofilms, but also the difficulty of this determination. The above described heterogeneity of biofilms may be a large source of error. Killing of the sample for observation may induce artifacts. D_b for small molecules, such as oxygen, nitrate, and glucose, can be assumed to be close to that of water, as biofilms and microbial mats can be considered as highly hydrated gels. For an extensive review on diffusion in gels, see Westrin (1991).

Diffusivities in biofilms have been determined from transient and steady state fluxes through biofilm in diffusion chambers and uptake experiments (i.e., on complete biofilms and mats disregarding the possibility of different transport rates through voids

and cell clusters or due to gradients in porosity and tortuosity; Revsbech, 1989; Glud et al., 1995). Alternatively, diffusion coefficients inside cell clusters have been determined by using microinjection of a nonreactive dye (De Beer et al., 1997b). After injection of a small aliquot (<1 nL), a fluorescent plume develops that expands and simultaneously fades in intensity due to dilution. At a fixed position from the injection point the concentration of the tracer will initially increase, followed by a decrease. The time-dependent distribution of the tracer is described by the equation (Crank, 1975)

$$c_r = 0.5\, c_i \left[\operatorname{erf}\left(\frac{r_a + r}{2\sqrt{Dt}} \right) + \operatorname{erf}\left(\frac{r_a - r}{2\sqrt{Dt}} \right) \right] - \frac{c_i}{r} \sqrt{\frac{Dt}{\pi}} \left[\exp\left(\frac{-(r_a - r)^2}{\sqrt{4Dt}} \right) - \exp\left(\frac{-(r_a + r)^2}{\sqrt{4Dt}} \right) \right] \quad (15.13)$$

where t is elapsed time, r is the radius of the plume, r_a is its initial radius, c_i is the initial concentration of the plume, D is the apparent diffusion coefficient, and erf(·) is the error function. By measuring the local fluorescence intensity as an indicator of the dye concentration (c_r), the apparent diffusion coefficient can be found by iterative fitting of equation (15.13).

The diffusion coefficient for small molecules (molecular weight, MW < 1000) in cell clusters has been found to be close to that in water. However, movement of large molecules (MW > 240000) seems to be impeded by the cell cluster matrix by about 60%. The latter phenomenon results from physical obstruction of molecular movement by the EPS matrix. Semiempirical relations (Westrin, 1991), applied to the diffusion data, suggest that the biofilm can be considered as a porous matrix with a pore diameter of 80–90 nm. This spacing is small enough to allow movement of nutrients but to trap cells. Such a matrix will not allow water flow; thus, in the absence of voids, diffusion is the only transport process in an EPS cemented biofilm. No microscopic technique to date can elucidate the structure of EPS, and the results from the diffusion experiment cannot be confirmed directly. In comparison, the top layer of a biofilm can be structured from filaments, forming a loose matrix of streamers. Liquid can flow through such a matrix liquid in a dispersed manner. Diffusion measurements indicate that this structure does not constitute a significant resistance to mass transport, as the substrate concentration remains close to that in the overlying liquid.

This exposé on diffusion in biofilms is valid only if the biomass does not change the porewater viscosity. The latter may be possible through the excretion of large amounts of organic polymers, primarily when exposed to extreme C:N ratios, osmotic stress, or other environmental stress factors. We have also largely ignored possible effects on solute transport from meiofaunal activity in biofilms and mats. A few studies point to a significant enhancement of transport by meiofauna activities (e.g., Sweerts et al. 1991; Aller and Aller, 1992), but more detailed studies on enhanced mass transfer by microscale faunal activity are still required.

15.3 New Approaches to Mass Transfer in Biofilms and Mats

Future studies of mass transfer and how it interacts with microbial processes in biofilms and microbial mats need to address the inherent heterogeneity of such biological systems in more detail. The microscopy techniques for flow and diffusion measurements, described above, can be performed only in the case of transparent matrices, as it requires microscopic observations of particles or plumes. This precludes their use in sediments and thick mats and biofilms. The same holds true for the methodology

known as fluorescence recovery after bleaching (FRAB), which is based on bleaching of a volume element with a strong laser light pulse and following the diffusion of a fluorescent dye from the surrounding area (Axelrod et al., 1976). We are currently experimenting with spin-echo nuclear magnetic resonance (NMR), which is a promising for the determination of diffusion coefficients in thick media. With 2D NMR imaging, it is possible to study sample heterogeneity with respect to diffusivity and water content, both in vertical and in lateral direction (A. Wieland et al., unpublished data). Moreover, the measurements are noninvasive, and no sample preparation is needed. In principle liquid flow can also be measured with this technique. However, flow velocities lower than 50 $\mu m\ s^{-1}$ were unmeasurable, which makes this technique insufficiently sensitive for most cases. A further disadvantage of microscopic and NMR techniques is that in situ measurements are currently impossible. Thus, more sensitive tools that can be used in the field are needed, and new flow/diffusion microsensors are under development for this purpose (see chapter 8).

While microsensors allow detailed study of DBLs and the distribution of important biogeochemical variables in biofilms and mats (see chapters 8 and 14), such investigations are inherently limited to point measurements. Furthermore, the mere insertion of microsensors into the DBL leads to a complex interaction between the thin sensor tip and the flow on a microscale; these can lead to a compression of the DBL and subsequent changes in the chemical gradients within biofilms and mats (Glud et al., 1994; Lorenzen et al., 1995). Thus, noninvasive techniques that allow for 2D or 3D mapping of the DBL should be developed. A recent technique that may allow such studies has been introduced by Glud et al. (1996), who employed optical planar sensor foils to map the 2D O_2 distribution in a sediment. By growing a thin biofilm on top of a sensor film, the 2D oxygen distribution at the bottom of the biofilm could be observed (Glud et al., 1998). While the heterogeneity of the oxygen distribution was similar to the one described from multiple microsensor measurements in section 15.2.3, a much more detailed picture of the oxygen dynamics and distribution could be obtained with the new planar sensor foils (fig. 15.8). Most recently, this technology has revealed the 2D distribution of photosynthetic activity and respiration in a microbial mat (R. N. Glud and M. Kühl, unpublished data).

Even in apparently simple systems, such as biofilms and microbial mats, mass-transfer processes are much more complex than initially believed. In both mats and biofilms, the boundary layer is not a flat layer that restricts 1D transport; instead, it has a complex geometry, and often a 3D approach is needed to describe transport. The use of a few parameters, for example, a diffusion coefficient for internal transport and a mass-transfer coefficient for transport in the boundary layer, may be insufficient to model transport phenomena in these systems. Big gaps still exist in our basic knowledge of the structure and processes in benthic mats and biofilms. The suite of new techniques described here and in other chapters of this book, will allow detailed studies of the structure, mass transfer, and microbial activity.

We are indebted to Rik Beeftink (Wageningen Agricultural University) and Baukje Ozinga for supply of photographs, to Prof. Simon P. P. Ottengraf (Technical University Eindhoven) for the mathematics of the DBL, to Ola Holby, Ronnie Glud (Max Planck Institute Marine Microbiology) and Jens Gundersen (University of Aarhus) for use of a deep-sea profile, to Dave Davies and Gill Geesey (Montana State University) for valuable information, and to the editors of this book for their patience and effort. Part of this work was supported by the Körber Foundation (Germany).

References

Aller, R. C., and Aller, J. Y. (1992) Meiofauna and solute transport in marine muds. Limnol. Oceanogr. 37, 1018–1033.

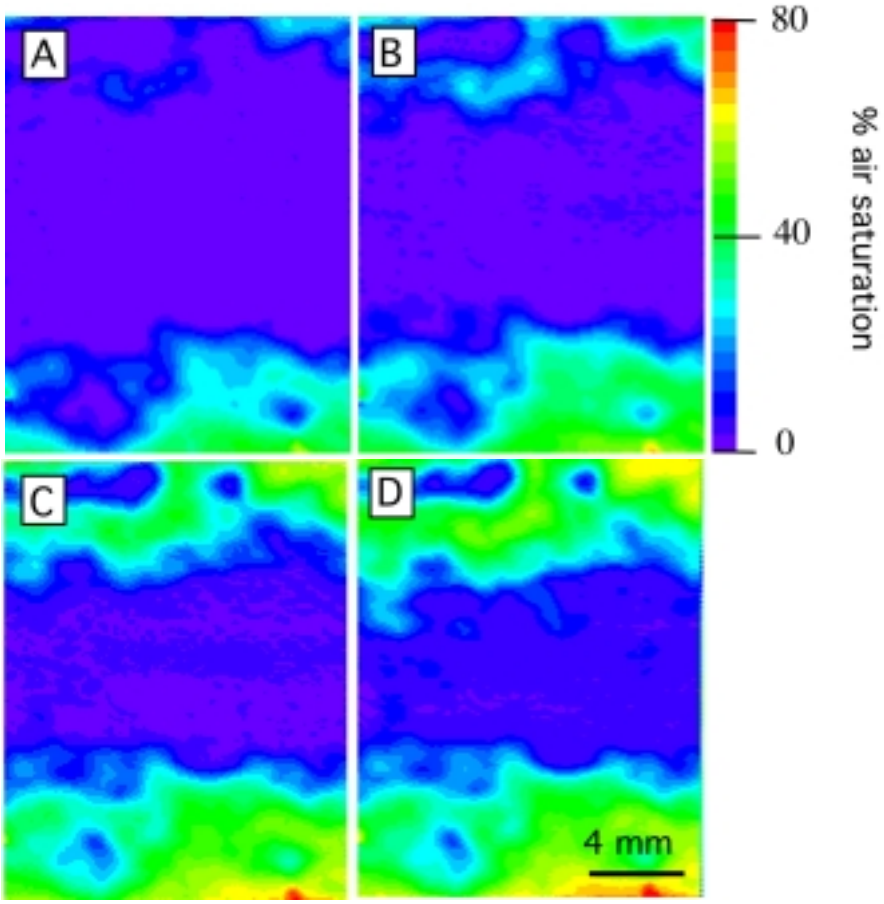

Figure 15.8 Oxygen images of the base of a 13-day-old biofilm at increasing u_∞, as recorded with a planar optode, i.e., A, 120.5 cm s^{-1}; B, 23.4 cm s^{-1}; C, 33.1 cm s^{-1}; and D, 35.1 cm s^{-1}. Color version available in the color insert of this book.

Allison, D. G., Evans, D. J., Brown, M. R. W., and P., G. (1990) Possible involvement of the division cycle in dispersal of *Escherichia coli* biofilms. Jour. Bact. 172, 1667–1669.

Axelrod, D., Koppel, D. E., Schlesinger, J., Elson, E., and Webb, W. W. (1976) Mobility measurement by analysis of fluorescence photobleaching recovery kinetics. Biophys. Jour. 16, 1055–1069.

Bailey, J. E., and Ollis, D. F. (1986) Biochemical Engineering Fundamentals, 2nd ed. McGraw-Hill, New York.

Beeftink, H. H., and Staugaard, P. (1986) Structure and dynamics of anaerobic bacterial aggregates in a gas-lift reactor. Appl. Environ. Microbiol. 52, 1139–1146.

Boudreau, B. P. (1997) Diagenetic Models and their Implementation. Springer-Verlag, Heidelberg.

Boudreau, B. P., and Westrich, J. T. (1984) The dependence of bacterial sulfate reduction on sulfate concentration in marine sediments. Geochim. Cosmochim. Acta 48, 2503–2516.

Bremer, P. J., Geesey, G. G., and Drake, B. (1992) Atomic force microscopy examnation

of the topography of a hydrated bacterial biofilm on a copper surface. Current Microbiol. 24, 223–230.
Canfield, D., and Des Marais, D. J. (1993) Biochemical cycles of carbon, sulfur, and free oxygen in a microbial mat. Geochim. Cosmochim. Acta 57, 3971–3984.
Canfield, D. E., and Des Marais, D. J. (1991) Aerobic sulfate reduction in microbial mats. Science 251, 1471–1473.
Characklis, W. G. and Marshall, K. C. (1989) Biofilms. Wiley, New York.
Chayen, J., Bitensky, L., and Butcher, R. (1973) Practical Histochemistry. Wiley, New York.
Christensen, B. E., and Characklis, W. G. (1990) Physical and chemical properties of biofilms, *in* Biofilms (Characklis, W. G., and Marshall, K. C., eds.), p. 93–130. Wiley and Sons.
Crank, J. (1975) The Mathematics of Diffusion, 2nd ed. Oxford University Press, New York.
Daffonchio, D., Thaveeshi, J., and Verstraete, W. (1995) Contact angle measurement and cell hydrofobicity of granular sludge from UASB reactors. Appl. Environ. Microbiol. 61, 3676–3680.
Davies, D. G., Parsek, M. R., Pearson, J. P., Iglewski, B. H., Costerton, J. W., and Greenberg, E. P. (1998) The involvement of cell-to-cell signals in the development of a bacterial biofilm. Science 280, 295–298.
De Beer, D., Glud, A., Epping, E., and Kühl, M. (1997a) A fast responding CO_2 microelectrode for profiling sediments, microbial mats and biofilms. Limnol. Oceanogr. 42, 1590–1600.
De Beer, D., and Stoodley, P. (1995) Relation between the structure of an aerobic biofilm and transport phenomena. Water Sci. Technol. 32, 11–18.
De Beer, D., Stoodley, P., and Lewandowski, Z. (1994a) Liquid flow in heterogeneous biofilms. Biotech. Bioeng. 44, 636–641.
De Beer, D., Stoodley, P., and Lewandowski, Z. (1997b) Measurement of local diffusion coefficients in biofilms by microinjection and confocal microscopy. Biotech. Bioeng. 53, 151–158.
De Beer, D., Stoodley, P., Roe, F., and Lewandowski, Z. (1994b) Effect of biofilm structures on oxygen distribution and mass transfer. Biotechn. Bioeng. 43, 1131–1138.
De Beer, D., van den Heuvel, J. C., and Ottengraf, S. P. P. (1993) Microelectrode measurements of the activity distribution in nitrifying bacterial aggregates. Appl. Environ. Microbiol. 59, 573–579.
Decho, A. W. (1990) Microbial exopolymer secretions in ocean environments: their role(s) in food webs and marine processes. Oceanogr. Mar. Biol. Ann. Rev. 28, 73–153.
Decho, A. W., and Lopez, G. R. (1993) Exopolymer microenvironments of microbial flora: multiple and interactive effects on trophic relationships. Limnol. Oceanogr. 38, 1633–1645.
Eighmy, T. T., Maratea, D., and Bishop, P. L. (1983) Electron microscopic examination of wastewater biofilm formation and structural components. Appl. Environ. Microbiol. 45, 1921–1931.
Fattom, A., and Shilo, M. (1984) Hydrophobicity as an adhesion mechanism of benthic cyanobacteria. Appl. Environ. Microbiol. 47, 135–143.
Frund, C., and Cohen, Y. (1992) Diurnal cycles of sulfate reduction under oxic conditions in Cyanobacterial mats. Appl. Environ. Microbiol. 58, 70–77.
Glud, R. N., Gundersen, J. K., Revsbech, N. P., and Jørgensen, B. B. (1994) Effects on the bentic diffusive boundary layer imposed by microelectrodes. Limnol. Oceanogr. 39, 462–467.
Glud, R. N., Jensen, K., and Revsbech, N. P. (1995) Diffusivity in surficial sediments and benthic mats determined by use of a combined N_2O-O_2 microsensor. Geochim. Cosmochim. Acta 59, 231–237.
Glud, R., Ramsing, N. B., Gundersen, J. K., and Klimant, I. (1996) Planar optrodes, a

new tool for finescale measurements of two dimensional O_2 distribution in bentic communities. Mar. Ecol. Progr. Series 140, 216–226.
Glud, R. N., Santegoeds, C. M., de Beer, D., Kohls, O., and Ramsing, N. B. (1998) Oxygen dynamics at the base of a biofilm studied with planar optodes. Aquat. Microbial Ecol. 14, 223–233.
Greenberg, E. P. (1997) Quorum sensing in gram-negative bacteria. ASM News 63, 371–377.
Griebe, T. (1991) Experimentelle Untersuchungen zur Aggregatbildung. Ph.D. thesis, University Hamburg.
Haugland, R. P. (1996) Handbook of fluorescent probes and research chemicals, 6th ed. Molecular Probes, Eugene.
Jørgensen, B. B. (1994) Diffusion processes and boundary layers in microbial mats, *in* Microbial Mats: Structure, Development and Environmental Significance, NATO ASI Series G 35 (Stal, L.J., and Caumette, P., eds.), p. 243–253. Springer-Verlag, Heidelberg.
Jørgensen, B. B., and Des Marais, D. (1990) The diffusive boundary layer of sediments: oxygen microgradients over a microbial mat. Limnol. Oceanogr. 35, 1343–1355.
Jørgensen, B. B., and Revsbech, N. P. (1985) Diffusive boundary layers and the oxygen uptake of sediments and detritus. Limnol. Oceanogr. 30, 111–122.
Karsten, U., and Kühl, M. (1996) Die Mikrobenmatte-das kleinste Ökosystem der Welt. Biol. Zeit 26, 16–26.
Krekeler, D., Sigalevich, P., Teske, A., Cohen, Y., and Cypionka, H. (1997) Desulfovibriae oxyclineae sp. nov., an oxygen-respiring sulfate-reducing bacterium from the oxic layer of a microbial mat from Solar Lake (Sinai). Archiv. Microbiol. 167, 369–375.
Kugaprasatham, S., Nagaoka, H., and Ohgaki, S. (1992) Effect of turbulence on nitrifying biofilms at non-limiting substrate conditions. Water Res. 26, 1629–1638.
Kühl, M., Glud, R. N., Plough, H., and Ramsing, N. B. (1996) Microenvironmental control of photosynthesis and photosynthesis coupled respiration in an epilithic cyanobacterial biofilm. Jour. Phycol. v. 32, 799-812.
Lawrence, J. R., Korber, D. R., Hoyle, B. D., Costerton, J. W., and D.E., C. (1991) Optical sectioning of microbial biofilms. Jour. Bact. 173, 6558–6567.
Libicki, S. B., Salmon, P. M., and Robertson, C. R. (1988) The effective diffusive permeability of a nonreacting solute in microbial cell aggregates. Biotech. Bioeng. 32, 68–85.
Little, B., Wagner, P., Ray, R., Pope, R., and Scheetz, R. (1991) Biofilms, an ESEM evaluation of artifacts introduced during preparation. Jour. Indus. Microbiol. 8, 213–222.
Lorenzen, J., Glud, R. N., and Revsbech, N. P. (1995) Impact of microsensor-caused changes in diffusive boundary layer thickness on O_2 profiles and photosynthetic rates in benthic communities of microorganisms. Mar. Ecol. Progr. Ser. 119, 237–241.
Mack, W. N., Mack, J. P., and Ackerson, A. O. (1975) Microbial film development in trickling filters. Microbial Ecol. 2, 215–316.
Massol-Deya, A. A., Whallon, J., Hickey, R. F., and Tiedje, J. M. (1995) Channel structure in aerobic biofilms of fixed-film reactors treating contaminated groundwater. Appl. Environ. Microbiol. 61, 769–777.
Nielsen, L. P., Christensen, P. B., Revsbech, N. P., and Sørensen, J. (1990) Denitrification and photosynthesis in stream sediment studied with microsensor and whole-core techniques. Limnol. Oceanogr. 35, 1135–1144.
Revsbech, N. P. (1989) Diffusion characteristics of microbial communities determined by use of oxygen microsensors. Jour. Microbiol. Meth. 9, 111–122.
Rittmann, B. E., and Manem, J. A. (1992) Development and experimental evaluation of a steady-state, multispecies biofilm model. Biotech. Bioeng. 39, 914–922.
Robinson, R. W., Akin, D. E., Nordstedt, R. A., Thomas, M. V., and Aldrich, H. C. (1984) Light and electron microscopic examinations of methane producing biofilms

from anaerobic fixed bed reactors. Appl. Environ. Microbiol. 48, 127–136.
Schlichting, H. (1968) Boundary Layer Theory. McGraw-Hill, New York.
Schmidt, J. E., and Ahring, B. K. (1994) Extracellular polymers in granular sludge from differen upflow anaerobic sludge blanket (UASB) reactors. Appl. Microbiol. Biotechnol. 42, 457–462.
Schopf, J. W., and Klein, C. (1992) The Proterozoic Biosphere - A Multidisciplinary Study. Cambridge University Press, Cambridge.
Shaw, D. A., and Hanratty, T. J. (1977) Turbulent mass transfer to a wall for large Schmidt numbers. Amer. Chem. Eng. Jour. 23, 28–37.
Stal, L. J., and Caumette, P. (1994) Microbial mats: structure, development and environmental significance. Springer-Verlag, Heidelberg.
Stewart, P. S., Drury, W. J.,, and Murga, R. (1993) Quantitative observations of heterogeneities in Pseudomonas aeruginosa biofilms. Appl. Environ. Microbiol. 59, 327–329.
Stewart, P. S., Murga, R., Srinivasan, R., and De Beer, D. (1995) Biofilm structural heterogeneity visualized by three microscopic methods. Water Res. 29, 2006–2009.
Sweerts, J.-P. R. A., Bar-Gillisen, M. J., Cornelise, A. A., and Cappenberg, T. E. (1991) Oxygen consuming processes at the profundal and littoral sediment-water interface of a small meso-eutrophic lake (lake Vechten, the Netherlands). Limnol. Oceanogr. 36, 1124–1133.
Tijhuis, L., Hijman, B., van Loosdrecht, M. C. M., and Heijnen, J. J. (1996) Influence of detachment, substrate loading and reactor scale on the formation of biofilms in airlift reactors. Appl. Microbiol. Biotechnol. 45, 7–17.
Wanner, O., and Gujer, W. (1986). A multispecies biofilm model. Biotechn. Bioeng. 28, 314–328.
Westrin, B. A. (1991). Diffusion Measurements in Gels. University of Lund.